


Particle hydrodynamics in acoustic fields: Unifying acoustophoresis with streaming

Xiaokang Zhang , Jake Minten, and Bhargav Rallabandi **Department of Mechanical Engineering, University of California, Riverside, California 92521, USA*

(Received 26 September 2023; accepted 12 March 2024; published 10 April 2024)

Acoustic fields are widely used to manipulate suspended particles, by rectifying the inertia of rapid oscillations into steady transport. We develop an analytic theory of this particle motion, systematically unifying inviscid acoustophoresis with viscous streaming effects. By applying the Lorentz reciprocal theorem, we obtain a Faxén-like relationship that relates particle motion to a generalized version of the secondary radiation force that depends on the thickness of the oscillatory Stokes layer around the particle, and the density and compressibility contrast between the particle and the fluid. The theory identifies a reversal of particle motion when inertial and viscous forces are comparable, which we validate quantitatively with numerical solutions of the timescale-separated hydrodynamics. We discuss the implications of our findings for practical applications seeking to sort or focus particles by size or material properties.

DOI: [10.1103/PhysRevFluids.9.044303](https://doi.org/10.1103/PhysRevFluids.9.044303)

I. INTRODUCTION AND PROBLEM SETUP

Acoustophoresis refers to the steady drift of suspended particles due to scattering of an incident acoustic field [1]. Acoustic fields—more generally, oscillatory flows—also drive a steady secondary “streaming” flow due to viscous effects, which transports suspended particles [2]. Both effects are produced by a nonlinear rectification of the inertia of rapid oscillations, and act in concert to transport suspended particles [3]. These effects have been used in a growing number applications to manipulate particles, cells, droplets, and microorganisms using ultrasound. Recent examples include the lysis of vesicles [4], microfluidic focusing and sorting [3,5], cell patterning [6,7], the design of microrobots [8], and the levitation of particles and droplets [9–12]. In these applications, inertial and viscous forces focus particles at nodes or antinodes of an acoustic standing wave [3], drive motion toward or away from solid surfaces and fluid interfaces [5,13,14], or assemble particles into chains or clusters [15–17].

To understand these phenomena, it is necessary to quantify the emergent time-averaged motion of the particles, driven by an interplay of acoustophoresis and streaming effects. The competition between viscous and inertial forces on the particle is quantified by the dimensionless parameter $\delta = \sqrt{2\nu}/(\omega a^2)$, which is the ratio of a viscous Stokes layer thickness $\sqrt{2\nu}/\omega$ to the particle radius a . Here, ν is the kinematic viscosity of the fluid and ω is the angular frequency of the sound (Fig. 1). The theory of secondary radiation forces (SRF) [18–20], widely used in acoustofluidics, addresses the high-frequency inviscid limit ($\delta \ll 1$) but neglects viscous effects and streaming. Recent work using the Gatignol-Maxey-Riley equation [21,22] (often with inertial modifications [14,23–25]) better captures transport by viscous streaming associated with $\delta \gg 1$, but neglects compressibility effects important in acoustics. At intermediate δ , where many experiments operate, the two formalisms are in disagreement, even over the direction of particle motion [20,24,26].

*bhargav@enr.ucr.edu

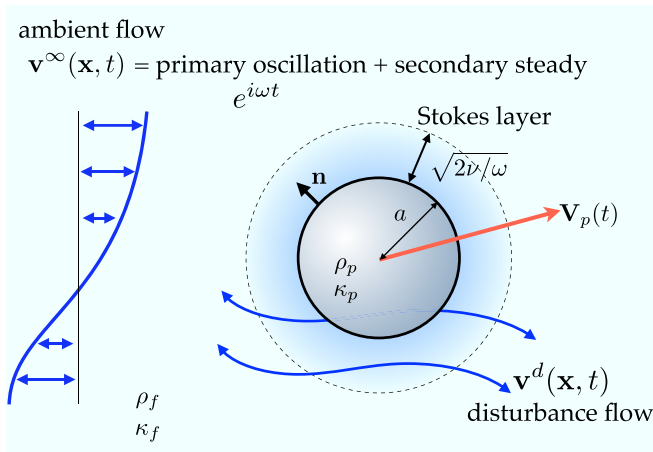


FIG. 1. Problem setup: An ambient fluid flow (density ρ_f , compressibility κ_f) produces oscillations of a suspended particle (density ρ_p , compressibility κ_p). Advective nonlinearities drive a secondary time-averaged motion of the particle.

Here, we develop an analytic theory of particle motion that spans the entire range of experimentally relevant parameters, systematically unifying the inviscid acoustofluidic and viscous streaming regimes. In the absence of the particle, the acoustic driving sets up a known “ambient” (or incident) fluid flow $\mathbf{v}^\infty(\mathbf{x}, t)$ (Fig. 1). The ambient flow is dominated by a fast and rapidly oscillating primary component of characteristic speed v and angular frequency ω , whose oscillation amplitude relative to the particle size is $\varepsilon = v/(a\omega)$. As is typical for acoustically driven systems, the ambient flow may also contain a slower secondary steady component (the “streaming” flow) that is quadratic in the sound amplitude and has a velocity scale εv .

A suspended particle responds to the ambient flow by translating with velocity $\mathbf{V}_p(t)$, which is a combination of an oscillatory response and a time-averaged drift. Additionally, the particle responds to the oscillating pressure of the ambient flow by executing volume oscillations with surface velocity $V_n(t)\mathbf{n}$ along the surface normal \mathbf{n} . This creates a disturbance (or “scattered”) flow $\mathbf{v}^d(\mathbf{x}, t)$, leading to a net flow $\mathbf{v} = \mathbf{v}^\infty + \mathbf{v}^d$. The fluid (f) and the particle (p) have equilibrium density $\rho_{f,p}$ and compressibility $\kappa_{f,p} = (\rho_{f,p}c_{f,p}^2)^{-1}$, where $c_{f,p}$ is the speed of sound in the respective medium. Scaling lengths with a , time with ω^{-1} , and defining a dimensionless density field $\varrho(\mathbf{x}, t) = \rho(\mathbf{x}, t)/\rho_f$, the flow is governed by

$$\frac{2}{\delta^2} \left(\frac{\partial \mathbf{v}}{\partial t} + \varepsilon \mathbf{v} \cdot \nabla \mathbf{v} \right) = \nabla \cdot \boldsymbol{\sigma}, \quad (1a)$$

$$\frac{\partial \varrho}{\partial t} + \varepsilon \nabla \cdot (\varrho \mathbf{v}) = 0, \quad (1b)$$

where $\boldsymbol{\sigma} = -p\mathbf{I} + (\nabla \mathbf{v} + \nabla \mathbf{v}^T)$ is the stress tensor (scaled with $\mu v/a$, where $\mu = \nu \rho_f$). The particle motion must be determined as part of the solution; of particular interest is time-averaged particle velocity (\mathbf{V}_p).

II. SMALL AMPLITUDE THEORY

While direct numerical simulations (DNS) of (1) are expensive, time-averaged inertial effects are quadratic in oscillation amplitude in the vast majority of applications [1,3,5,13,17]. We focus on these quadratic effects, fully resolving them in a nonlinear theory for small amplitude $\varepsilon \ll 1$. (More precisely, the amplitude of particle oscillation relative to the fluid must be small.) We

seek a perturbation solution with $(\mathbf{v}, \boldsymbol{\sigma}) \sim (\mathbf{v}_1, \boldsymbol{\sigma}_1) + \varepsilon(\mathbf{v}_2, \boldsymbol{\sigma}_2)$ and $\varrho \sim 1 + \varepsilon\varrho_1$, where primary components (subscript 1) oscillate with frequency ω , and secondary components (subscript 2) involve steady terms that are of practical interest. Separating orders of ε (equivalently, separating fast and slow timescales) in (1) leads to [1,26]

$$\frac{2}{\delta^2} \frac{\partial \mathbf{v}_1}{\partial t} = \nabla \cdot \boldsymbol{\sigma}_1, \quad \frac{\partial \varrho_1}{\partial t} + \nabla \cdot \mathbf{v}_1 = 0, \quad (2a)$$

$$\nabla \cdot \left\langle \boldsymbol{\sigma}_2 - \frac{2}{\delta^2} \mathbf{v}_1 \mathbf{v}_1 \right\rangle = \mathbf{0}, \quad \nabla \cdot \langle \mathbf{v}_2 + \varrho_1 \mathbf{v}_1 \rangle = 0, \quad (2b)$$

where angle brackets define a time average over an oscillation according to $\langle g \rangle(\mathbf{x}) = (2\pi)^{-1} \int_t^{t+2\pi} g(\mathbf{x}, t) dt$ and isolate steady flow features. Pressure and density oscillations are related by $p_1 = \varrho_1 / (\kappa_f \mu \omega)$. The perturbative approach is uniformly valid to the order of ε considered here (velocity $\propto \varepsilon^2$), and inertial far-field effects are negligible (Appendix A).

The flow satisfies no slip ($\mathbf{v} = \mathbf{V}_p + V_n \mathbf{n}$) on the instantaneous particle surface $S_p(t)$. We project this condition onto the time-averaged surface $\langle S_p \rangle$ and separate powers of ε (Appendix B) to obtain effective boundary conditions for the primary and secondary flow

$$\mathbf{v}_1 = \mathbf{V}_{p1} + \mathbf{V}_{n1} \mathbf{n} \quad \text{on} \quad \langle S_p \rangle, \quad (3a)$$

$$\langle \mathbf{v}_2 \rangle = \left\langle \mathbf{V}_{p2} - \int \mathbf{v}_1 dt \cdot \nabla \mathbf{v}_1 \right\rangle \quad \text{on} \quad \langle S_p \rangle, \quad (3b)$$

where \mathbf{V}_{p1} and V_{n1} denote translational and volumetric oscillations of the particle, while $\langle \mathbf{V}_{p2} \rangle = \varepsilon^{-1} \langle \mathbf{V}_p \rangle$ is the rescaled time-averaged particle velocity. Observe that (3b) involves a ‘‘Stokes drift’’ term, $\langle \int \mathbf{v}_1 dt \cdot \nabla \mathbf{v}_1 \rangle$, that arises naturally because the particle defines a material surface (Appendix B).

A. Oscillatory primary flow

The oscillatory primary flow around the particle is well known [27], so we only outline the main ideas. We make the ansatz that primary flow quantities oscillate as $\text{Re}[g(\mathbf{x})e^{it}]$ for generally complex $g(\mathbf{x})$. We focus on particles that are small relative to a spatial length scale L , of the ambient flow, typically either the wavelength of sound L_c or an external geometric scale L_g . Defining a local inertial frame $\mathbf{r} = \mathbf{x} - \langle \mathbf{X}_p \rangle$ relative to the time-averaged particle center $\langle \mathbf{X}_p \rangle$, we thus Taylor expand the ambient flow as

$$\mathbf{v}_1^\infty(\mathbf{x}, t) \sim \mathbf{V}_1^\infty(t) + \mathbf{E}_1^\infty(t) \cdot \mathbf{r} + \frac{1}{3} \Delta_1^\infty(t) \mathbf{r} + \dots \quad (4)$$

in terms of the velocity \mathbf{V}_1^∞ , the deviatoric rate of strain (extension rate) \mathbf{E}_1^∞ , and the velocity divergence (dilatation rate) Δ_1^∞ of the ambient flow, all evaluated at the average particle center $\langle \mathbf{X}_p \rangle$. These flow properties are complex phasors, and it will be understood that only the real part of any complex equality is physically meaningful. We neglect the rotation of the particle and the vorticity of the ambient flow, as they are typically small for spheres in acoustic fields [27].

The particle responds by producing an oscillatory disturbance flow \mathbf{v}_1^d . This disturbance decays on the scale of $a \ll L_c$ and is thus approximately incompressible [27]. The solution to the primary disturbance flow around the particle can then be written in terms of tensor harmonics [27–29] as (rewriting results from [20,27])

$$\mathbf{v}_1^d = \mathbf{D} \cdot (\mathbf{V}_{p1} - \mathbf{V}_1^\infty) + \mathcal{Q} : \mathbf{E}_1^\infty + \mathbf{m} \left(V_{n1} - \frac{\Delta_1^\infty}{3} \right). \quad (5)$$

Here, $\mathbf{m}(\mathbf{r})$, $\mathbf{D}(\mathbf{r}, \delta)$, and $\mathcal{Q}(\mathbf{r}, \delta)$ are monopole, dipole, and quadrupole tensors given by (defining $R = \lambda r$)

$$\mathbf{m}(\mathbf{r}) = \frac{\mathbf{r}}{r^3}, \quad (6a)$$

$$\mathbf{D}(\mathbf{r}, \lambda) = d_1 \left[\frac{\mathbf{I}}{r^3} - 3 \frac{\mathbf{r}\mathbf{r}}{r^5} \right] + d_2 \left[e^{-R} \left(\frac{1}{R} + \frac{1}{R^2} + \frac{1}{R^2} \right) \mathbf{I} - \frac{e^{-R}}{r^2} \left(\frac{1}{R} + \frac{3}{R^2} + \frac{3}{R^2} \right) \mathbf{r}\mathbf{r} \right], \quad (6b)$$

$$\mathcal{Q}(\mathbf{r}, \lambda) = q_1 \left[6 \frac{\mathbf{I}}{r^5} - 15 \frac{\mathbf{r}\mathbf{r}}{r^7} \right] + q_2 \left[\frac{e^{-R}}{r^2} \left(1 + \frac{3}{R} + \frac{6}{R^2} + \frac{6}{R^3} \right) \mathbf{I} - \frac{e^{-R}}{r^4} \left(1 + \frac{6}{R} + \frac{15}{R^2} + \frac{15}{R^3} \right) \mathbf{r}\mathbf{r} \right]. \quad (6c)$$

No-slip conditions on the mean particle surface ($r = 1$) determine the coefficients

$$d_1 = -\frac{3 + 3\lambda + \lambda^2}{2\lambda^2}, \quad d_2 = \frac{3e^\lambda \lambda}{2}, \quad q_1 = \frac{15 + 15\lambda + 6\lambda^2 + \lambda^3}{9\lambda^2(1 + \lambda)}, \quad \text{and} \quad q_2 = -\frac{5e^\lambda \lambda}{3(1 + \lambda)}. \quad (7)$$

The primary oscillatory flow $\mathbf{v}_1 = \mathbf{v}_1^\infty + \mathbf{v}_1^d$ and the associated stress $\boldsymbol{\sigma}_1$ are now known in terms of the yet-to-be-determined oscillatory particle kinematics \mathbf{V}_{p1} and V_{n1} . To determine \mathbf{V}_{p1} , we invoke conservation of the particle momentum (projected on e^{it} modes), $\frac{4}{3}\pi a^3 \rho_p \frac{d\mathbf{V}_{p1}}{dt} = \int_{(S_p)} \mathbf{n} \cdot \boldsymbol{\sigma}_1 dS$, to obtain [20]

$$\mathbf{V}_{p1} - \mathbf{V}_1^\infty = \mathcal{R}\mathbf{V}_1^\infty, \quad \text{where} \quad \mathcal{R}(\delta, \tilde{\rho}) = -\frac{2\lambda^2(\tilde{\rho} - 1)}{\lambda^2(2\tilde{\rho} + 1) + 9\lambda + 9}, \quad (8a)$$

a relative oscillatory Stokes particle mobility, where $\tilde{\rho} = \rho_p/\rho_f$ is the density ratio and $\lambda = (1 + i)/\delta$. The real and imaginary parts of \mathcal{R} , respectively, quantify in-phase and out-of-phase oscillations of the particle relative to the fluid. Equilibrium of normal stresses on the particle surface determines $V_{n1} = \frac{1}{3}(\tilde{\kappa} - 1)\Delta_1^\infty$, where $\tilde{\kappa} = \kappa_p/\kappa_f$ is the compressibility ratio [20].

B. Time-averaged secondary force

Having fully determined the primary flow \mathbf{v}_1 , we turn to the time-averaged particle motion. Doinikov [26] showed that the time-averaged force exerted by the fluid on the particle (in units of $\varepsilon\mu a v$) is $\langle \mathbf{F} \rangle = \int_{(S_p)} \mathbf{n} \cdot \left\langle \boldsymbol{\sigma}_2 - \frac{2}{\delta^2} \mathbf{v}_1 \mathbf{v}_1 \right\rangle$. The ambient flow makes no contribution to the time-averaged force as it satisfies (2b) everywhere (in particular also inside the particle volume). Thus, we can write the force as

$$\langle \mathbf{F} \rangle = \int_{(S_p)} \mathbf{n} \cdot \left\langle \boldsymbol{\sigma}_2 - \frac{2}{\delta^2} \mathbf{v}_1 \mathbf{v}_1 \right\rangle^d dS, \quad (9)$$

where we recall that the superscript d denotes disturbance contributions due to the particle, defined for any field g by $g^d = g - g^\infty$. Evaluating (9) entails finding $\boldsymbol{\sigma}_2^d$ in the course of solving for the (analytically intractable) secondary flow.

1. Reciprocal relation for the time-averaged force

We use the Lorentz reciprocal theorem [30,31] to develop analytic insight into the time-averaged force without resolving the details of the secondary flow. We first introduce the steady Stokes flow around by a sphere translating with velocity $\hat{\mathbf{V}}$ through quiescent fluid [flow velocity $\hat{\mathbf{v}}(\mathbf{x})$, stress $\hat{\boldsymbol{\sigma}}(\mathbf{x})$]. This flow (which we call the auxiliary flow) satisfies

$$\nabla \cdot \hat{\boldsymbol{\sigma}} = \mathbf{0}, \quad \nabla \cdot \hat{\mathbf{v}} = 0, \quad \text{subject to} \quad \hat{\mathbf{v}}|_{(S_p)} = \hat{\mathbf{V}}, \quad \hat{\mathbf{v}}|_{r \rightarrow \infty} = \mathbf{0}. \quad (10)$$

The rate of strain and surface traction of the auxiliary flow are, respectively, $\hat{\mathbf{E}} = \mathcal{E}(\mathbf{x}) \cdot \hat{\mathbf{V}}$ and $\mathbf{n} \cdot \hat{\boldsymbol{\sigma}}|_{(S_p)} = \mathbf{T}(\mathbf{x}) \cdot \hat{\mathbf{v}}$, where the tensors \mathcal{E} and \mathbf{T} are (using indices for clarity) [28,32]

$$\mathcal{E}_{ijk} = \frac{3}{4} \left[\left(\frac{\delta_{ij} r_k}{r^3} - 3 \frac{r_i r_j r_k}{r^5} \right) + \frac{1}{3} \left(-3 \frac{r_i \delta_{jk}}{r^5} - 3 \frac{r_j \delta_{ik}}{r^5} - 3 \frac{\delta_{ij} r_k}{r^5} + 15 \frac{r_i r_j r_k}{r^7} \right) \right], \quad \text{and} \quad T_{ij} = -\frac{3}{2} \delta_{ij}. \quad (11)$$

We use (2b) and (10) to construct the symmetry relation $\nabla \cdot \langle \boldsymbol{\sigma}_2 - \frac{2}{\delta^2} \mathbf{v}_1 \mathbf{v}_1 \rangle^d \cdot \hat{\mathbf{v}} = \nabla \cdot \hat{\boldsymbol{\sigma}} \cdot \langle \mathbf{v}_2 \rangle^d$, which, upon rearranging, yields

$$\nabla \cdot \left(\left\langle \boldsymbol{\sigma}_2 - \frac{2}{\delta^2} \mathbf{v}_1 \mathbf{v}_1 \right\rangle^d \cdot \hat{\mathbf{v}} \right) + \frac{2}{\delta^2} \langle \mathbf{v}_1 \mathbf{v}_1 \rangle^d : \hat{\mathbf{E}} = \nabla \cdot (\hat{\boldsymbol{\sigma}} \cdot \mathbf{v}_2^d) + \hat{p} (\nabla \cdot \langle \mathbf{v}_2 \rangle^d). \quad (12)$$

We then integrate over the volume $\langle V \rangle$ surrounding the time-averaged particle surface, apply the divergence theorem, and use (2b) and (10) once more to obtain

$$\int_{\langle S_p \rangle} \mathbf{n} \cdot \left\langle \boldsymbol{\sigma}_2 - \frac{2}{\delta^2} \mathbf{v}_1 \mathbf{v}_1 \right\rangle^d \cdot \hat{\mathbf{v}} dS = \int_{\langle S_p \rangle} \mathbf{n} \cdot \hat{\boldsymbol{\sigma}} \cdot \mathbf{v}_2^d dS + \int_{\langle V \rangle} \frac{2}{\delta^2} \langle \mathbf{v}_1 \mathbf{v}_1 \rangle^d : \hat{\mathbf{E}} dV + \int_{\langle V \rangle} \hat{p} \langle \mathbf{v}_1 \cdot \nabla \varrho_1 \rangle^d dV. \quad (13)$$

The first term of (13) is exactly equal to $\langle \mathbf{F} \rangle \cdot \hat{\mathbf{V}}$ due to (9), while its last term is smaller than the others by a factor of $(a/L_c)^2 \ll 1$ and is neglected (this is equivalent to the approximation $\nabla \cdot \langle \mathbf{v}_2^d \rangle \approx 0$). Next, we separate (3b) into ambient and disturbance contributions and find that $\langle \mathbf{v}_2 \rangle^d = \langle \mathbf{V}_{p2} \rangle - \langle \mathbf{v}_2^\infty + \int \mathbf{v}_1^\infty dt \cdot \nabla \mathbf{v}_1^\infty \rangle - \langle \int \mathbf{v}_1 dt \cdot \nabla \mathbf{v}_1 \rangle^d$ on $\langle S_p \rangle$. We see that the ambient ‘‘Lagrangian streaming’’ $\langle \mathbf{v}_L^\infty \rangle(\mathbf{x}) \stackrel{\text{def}}{=} \langle \mathbf{v}_2^\infty + \int \mathbf{v}_1^\infty dt \cdot \nabla \mathbf{v}_1^\infty \rangle$, which describes the time-averaged motion of a material element in the absence of the particle [2] (and is therefore a known quantity), arises naturally in the analysis. Eliminating the arbitrary auxiliary particle velocity $\hat{\mathbf{V}}$, (13) thus yields

$$\langle \mathbf{F} \rangle = \int_{\langle S_p \rangle} \langle \mathbf{V}_{p2} - \mathbf{v}_L^\infty \rangle \cdot \mathbf{T} dS - \int_{\langle S_p \rangle} \left\langle \int \mathbf{v}_1 dt \cdot \nabla \mathbf{v}_1 \right\rangle^d \cdot \mathbf{T} dS + \int_{\langle V \rangle} \frac{2}{\delta^2} \langle \mathbf{v}_1 \mathbf{v}_1 \rangle^d : \mathcal{E} dV. \quad (14)$$

2. Time-averaged particle motion and the generalized secondary radiation force

The result (14) is an exact reformulation of (9) for particles much smaller than the wavelength of sound. Notably, (14) only involves the primary flow \mathbf{v}_1 (which we have already determined), the ambient Lagrangian flow $\langle \mathbf{v}_L^\infty \rangle$ (which is known), and the secondary particle velocity $\langle \mathbf{v}_{p2} \rangle$ (which is the main quantity of interest). Evaluating (14) analytically yields (reverting to dimensional variables)

$$\langle \mathbf{F} \rangle = -6\pi\mu a \left[\langle \mathbf{V}_p \rangle - \left(1 + \frac{a^2}{6} \nabla^2 \right) \langle \mathbf{v}_L \rangle^\infty |_{\langle \mathbf{x}_p \rangle} \right] + \mathbf{F}^{\text{SR}}, \quad \text{where} \quad (15a)$$

$$\mathbf{F}^{\text{SR}} = \int_{\langle S_p \rangle} \left\langle \int \mathbf{v}_1 dt \cdot \nabla \mathbf{v}_1 \right\rangle^d \cdot \mathbf{T} dS + \int_{\langle V \rangle} \frac{2}{\delta^2} \langle \mathbf{v}_1 \mathbf{v}_1 \rangle^d : \mathcal{E} dV. \quad (15b)$$

The first term of (15a) is a Stokes drag with a Faxén correction for a particle moving through the ambient Lagrangian streaming field $\langle \mathbf{v}_L \rangle^\infty$. The second term, \mathbf{F}^{SR} is a time-averaged inertial force that can be interpreted as the generalization of the SRF for arbitrary δ , $\tilde{\kappa}$, and $\tilde{\rho}$. We observe that \mathbf{F}^{SR} is produced explicitly as a consequence of the oscillatory disturbance flow due to the particle.

We evaluate \mathbf{F}^{SR} analytically (using Mathematica), noting that the time-average of a product of two oscillating quantities $A(t) = \text{Re}[\alpha e^{it}]$ and $B(t) = \text{Re}[\beta e^{it}]$, with complex α and β , is $\langle AB \rangle = \frac{1}{2} \text{Re}[\alpha^* \beta] = \frac{1}{2} \text{Re}[\alpha \beta^*]$. The generalized SRF contains contributions from both extension and dilatation rates, and takes the form (defining $m_f = \frac{4}{3} \pi a^3 \rho_f$)

$$\mathbf{F}^{\text{SR}} = m_f \text{Re} \left[(\mathbf{V}_1^\infty)^* \cdot \mathbf{E}_1^\infty \mathcal{F}_E + (\mathbf{V}_1^\infty)^* \Delta_1^\infty \mathcal{F}_\Delta \right], \quad (16)$$

where $\mathcal{F}_E(\delta, \tilde{\rho})$ and $\mathcal{F}_\Delta(\delta, \tilde{\rho}, \tilde{\kappa})$ are complex coefficients that we discuss shortly, and where the asterisk denotes a complex conjugate. We note that the dilatation is related to the primary pressure by $\Delta^\infty = -i\omega\kappa_f p_1^\infty$, and for acoustic flows, it is often useful to write $(\mathbf{V}_1^\infty)^* \Delta_1^\infty = -\frac{\kappa_f}{\rho_f} p_1^\infty (\nabla p_1^\infty)^*$. If one interprets $\mathbf{V}_1^\infty(t)$, $\mathbf{E}_1^\infty(t)$, and $\Delta_1^\infty(t)$ as real oscillating quantities (rather than phasors), one

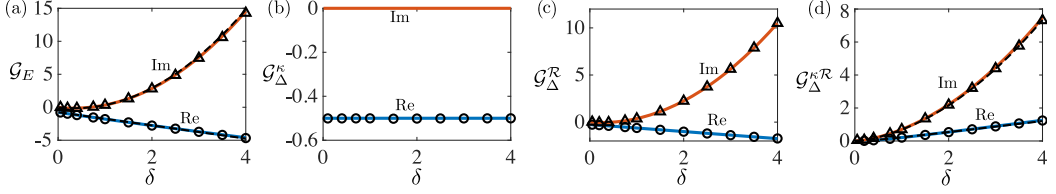


FIG. 2. Coefficients (a) \mathcal{G}_E , (b) $\mathcal{G}_\Delta^\kappa$, (c) \mathcal{G}_Δ^R , and (d) $\mathcal{G}_\Delta^{\kappa R}$ as obtained from the theory (curves) and from numerical solutions (symbols), showing real and imaginary parts. Approximations 19(a) and 19(d) are indicated by dashed curves in panels (a) and (d).

can equivalently write (16) as

$$\mathbf{F}^{\text{SR}} = 2m_f \left[\langle \mathbf{V}_1^\infty \cdot \mathbf{E}_1^\infty \rangle \text{Re}[\mathcal{F}_E] - \left\langle \frac{\partial \mathbf{V}_1^\infty}{\partial t} \cdot \mathbf{E}_1^\infty \right\rangle \frac{\text{Im}[\mathcal{F}_E]}{\omega} + \langle \mathbf{V}_1^\infty \Delta_1^\infty \rangle \text{Re}[\mathcal{F}_\Delta] - \left\langle \frac{\partial \mathbf{V}_1^\infty}{\partial t} \Delta_1^\infty \right\rangle \frac{\text{Im}[\mathcal{F}_\Delta]}{\omega} \right]. \quad (17)$$

The coefficients \mathcal{F}_E and \mathcal{F}_Δ are complex, and their real (imaginary) parts characterize inertial forces due to velocities oscillating in phase (out of phase) with rates of strain, as is made explicit by (17). They admit the decomposition

$$\mathcal{F}_E = \mathcal{R}^* \mathcal{G}_E, \quad (18a)$$

$$\mathcal{F}_\Delta = (\tilde{\kappa} - 1) \mathcal{G}_\Delta^\kappa + \mathcal{R}^* \mathcal{G}_\Delta^R + (\tilde{\kappa} - 1) \mathcal{R}^* \mathcal{G}_\Delta^{\kappa R}, \quad (18b)$$

into terms that depend on the density contrast ($\tilde{\rho} - 1$) through \mathcal{R}^* [see (8)], the compressibility contrast ($\tilde{\kappa} - 1$), or a combination. The associated complex coefficients $\mathcal{G}_A^B(\delta)$ are purely hydrodynamic quantities (independent of particle properties) that result from analytic evaluation of the integrals in (14) (using Mathematica) and are indicated as solid curves in Fig. 2. Simple analytic expressions for these coefficients are given by [recalling that $\lambda = (1 + i)/\delta$]

$$\mathcal{G}_E(\delta) \simeq -\frac{3\lambda^2 + \frac{4}{5}(1 + 9i)\lambda + 9}{4\lambda^2}, \quad (19a)$$

$$\mathcal{G}_\Delta^\kappa(\delta) = -\frac{1}{2}, \quad (19b)$$

$$\mathcal{G}_\Delta^R(\delta) = -\frac{\lambda^2 + 3i\lambda + 6}{4\lambda^2}, \quad (19c)$$

$$\mathcal{G}_\Delta^{\kappa R}(\delta) \simeq -\frac{15}{4\lambda^2} \frac{(9\lambda + 8i)}{(9\lambda + 40i)}. \quad (19d)$$

Note that (19b) and (19c) are exact. The approximations (19a) and (19d) are constructed to be asymptotic to the exact expressions (Appendix C) to leading order for both small and large δ . These approximations are indicated as dashed curves in Figs. 2(a) and 2(d) and are excellent representations of the exact results (accurate to within 3%; see Fig. 5) for all δ .

The relations (15)–(19) describe in full the time-averaged motion of a particle suspended in an oscillatory gradient flow and form the main result of this work. The theory generalizes the notion of SRF and unifies it with streaming, thus bridging inviscid acoustofluidics with viscous particle hydrodynamics. In many situations, the particle is freely suspended and is thus force free ($\langle \mathbf{F} \rangle = \mathbf{0}$), so (15) yields the time-averaged particle velocity]:

$$\langle \mathbf{V}_p \rangle = \left(1 + \frac{a^2}{6} \nabla^2 \right) \mathbf{v}_L^\infty \Big|_{\langle \mathbf{x}_p \rangle} + \frac{\mathbf{F}^{\text{SR}}}{6\pi\mu a}. \quad (20)$$

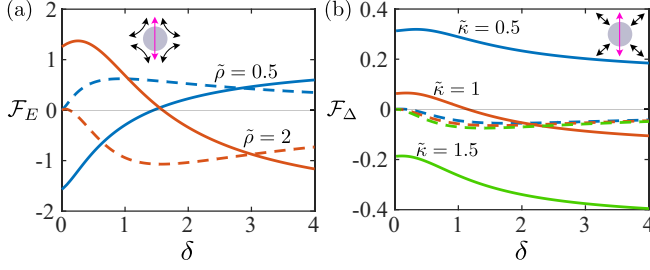


FIG. 3. Coefficients (a) \mathcal{F}_E and (b) \mathcal{F}_Δ versus the Stokes layer thickness $\delta = (\frac{2\nu}{a^2\omega})^{1/2}$. The real (solid) and imaginary (dashed) parts are due to velocities that are, respectively, in phase and out of phase with strain rates. \mathcal{F}_E reverses with δ for all $\tilde{\rho}$, while \mathcal{F}_Δ (here plotted for $\tilde{\rho} = 1.5$) reverses with δ for small compressibility contrasts ($\tilde{\kappa}$ close to unity).

In the limit $\delta \ll 1$, the present formulation fully recovers inviscid acoustofluidics [20], while the viscous limit recovers particle transport by streaming, with additional Faxén and inertial corrections; cf. [33]. Rectified inertial forces due to the second gradient of velocity (see [34,35]) are smaller by a relative factor of $O(a^2/L^2)$ and have been neglected here, but can be simply added to \mathbf{F}^{SR} .

The coefficient \mathcal{F}_E , associated with the rate of extension, is nonzero only for density-mismatched particles [Fig. 3(a)]. In the inviscid limit ($\delta \ll 1$), $\mathcal{F}_E \sim \mathcal{F}_E^{\text{inv}} = \frac{3(\tilde{\rho}-1)}{2(2\tilde{\rho}+1)}$ and in the viscous limit ($\delta \gg 1$), $\mathcal{F}_E \sim \mathcal{F}_E^{\text{visc}} = -\frac{(\tilde{\rho}-1)}{2}$, in agreement with [25]. Notably, these limits have opposite signs, so \mathcal{F}_E must reverse with δ . This reversal occurs around $\delta \approx 1.5$ for modest density contrasts [Fig. 3(a)] when viscous and inertial effects around the particle are comparable. This coincides with in-phase and out-of-phase oscillations of the particle (real and imaginary parts of \mathcal{R}) becoming of similar magnitude. The imaginary part of \mathcal{F}_E vanishes in both limits and is maximum at intermediate δ . Both real (in-phase) and imaginary (out-of-phase) parts of \mathcal{F}_E are comparable for the $O(1)$ values of δ typical of applications so both are likely important in practice.

The dilatation coefficient \mathcal{F}_Δ depends on three parameters (δ , $\tilde{\rho}$, and $\tilde{\kappa}$) and is plotted in Fig. 3(b). As with \mathcal{F}_E , \mathcal{F}_Δ has real-valued asymptotes in both inviscid ($\mathcal{F}_\Delta^{\text{inv}} = \frac{(\tilde{\rho}-1)}{2(2\tilde{\rho}+1)} - \frac{\tilde{\kappa}-1}{2}$) and viscous ($\mathcal{F}_\Delta^{\text{visc}} = -\frac{\tilde{\rho}-1}{3} - \frac{(\tilde{\kappa}-1)(\tilde{\rho}+2)}{6}$) limits. For fixed $\tilde{\rho}$, the main effect of varying $\tilde{\kappa}$ is to “shift” \mathcal{F}_Δ by a constant (this is due to the $\mathcal{G}_\Delta^{\text{K}}$ term). \mathcal{F}_Δ may also change sign with δ , but whether or not this reversal occurs is sensitive to both $\tilde{\kappa}$ and $\tilde{\rho}$. For particles with a moderate density contrast, \mathcal{F}_Δ reverses for $\tilde{\kappa}$ close to unity [Fig. 3(b)], while the reversal occurs over a wider range of $\tilde{\kappa}$ for particles with greater density contrast.

C. Time-averaged secondary flow

We verify the analytic predictions of the theory by developing numerical solutions of the detailed flow under the small-amplitude perturbation scheme, (2) and (3). While not a DNS of (1), this approach captures the practically relevant inertial effects in acoustofluidics, which are quadratic in oscillation amplitude [1]. We numerically solve (2b) with (3b), using the analytically determined (exact) oscillatory flow \mathbf{v}_1 discussed in Sec. II A. We focus on an axisymmetric setting, which suffices to capture all flow features associated with the time-averaged force discussed above, viz. translation, extension, and dilatation. As noted earlier, the disturbance flow is approximately incompressible up to corrections of $O(a^2/L_c^2)$. We thus utilize a vorticity-stream function formulation of (2b), written in spherical coordinates, which we solve numerically using finite differences.

To focus on the flow associated with the SRF (as opposed to that due to the time-averaged motion of the particle or the response to the steady Lagrangian ambient flow), we set $\langle \mathbf{V}_p \rangle = \mathbf{v}_{2L}^\infty = \mathbf{0}$, see (15). On solving for the secondary flow, we use (9) to calculate $\langle \mathbf{F} \rangle$, which isolates the generalized SRF \mathbf{F}^{SR} under the setup described above. Furthermore, by constructing oscillatory ambient flows

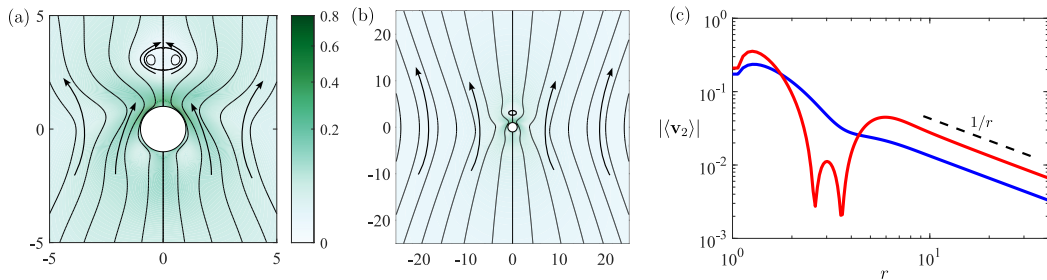


FIG. 4. Time-averaged disturbance flow $\langle \mathbf{v}_2 \rangle$ with $\delta = 1$ and $\tilde{\rho} = \tilde{\kappa} = 2$. The flow is axisymmetric about the polar axis \mathbf{p} , and the ambient flow corresponds to $\mathbf{V}_1^\infty = \mathbf{p} e^{it}$, $\mathbf{E}_1^\infty = \frac{1}{2}(-\mathbf{I} + 3\mathbf{p}\mathbf{p}) e^{it}$, $\Delta_1^\infty = e^{it}$, and $\mathbf{V}_{p2} = \mathbf{v}_{2L}^\infty = \mathbf{0}$. Panel (a) shows streamlines close to the particle, and (b) shows the same flow at greater length scales, revealing the behavior to be akin to a Stokeslet flow. Colors indicate dimensionless flow speed. (c) The speed of the secondary flow decays as r^{-1} , and can be seen here at locations along the axis of symmetry (red) and 90° from the axis of symmetry (blue).

with specific pairs of flow modes, we identify the computed force with a single term in (18). For example, a simulation with $\Delta_1^\infty = 0$ and nonzero \mathbf{V}_1^∞ and \mathbf{E}_1^∞ identifies \mathcal{G}_E . We repeat this procedure for different pairs of flow modes, extracting all four \mathcal{G} coefficients from numerical solutions. These numerically calculated coefficients (symbols in Fig. 2) are in excellent agreement with the analytic theory (19).

The numerical solutions also provide additional qualitative and quantitative insight that is not directly obtained through the reciprocal theorem. Figure 4(a) shows example streamlines of the numerically computed secondary axisymmetric flow for $\delta = 1$, with $\tilde{\rho} = \tilde{\kappa} = 2$. The flow is quite complex near the particle, including multiple stagnation and recirculation regions. However, far away from the particle, the secondary flow approaches that driven by a point force in Stokes flow, and exhibits the characteristic r^{-1} velocity decay of a Stokeslet flow [Figs. 4(b) and 4(c)]. As with a Stokeslet flow, the secondary flow speed at locations along the axis of the point force is twice that of the velocity at locations transverse to the axis [Fig. 4(c)]. Interestingly, however, the associated point force is distinct from \mathbf{F}^{SR} , as a part of the secondary stress (viz., the radiation pressure) is in hydrostatic balance (in the time-averaged sense) with the isotropic part of the Reynolds stress $\langle 2\delta^{-2}|\mathbf{v}_1|^2 \rangle$ and does not engender a secondary flow. Thus, the secondary flow is Stokes-like [as should be expected from (2b)] but involves additional complexities associated with inertial effects. A detailed analysis of these features is left to future work.

III. CONCLUSIONS

We conclude by discussing some ramifications and applications of the theory. For incompressible systems, the reversal of \mathcal{F}_E with δ indicates that large and small particles should exhibit qualitatively different behaviors when exposed to the same flow. For example, consider the incompressible radial flow driven by an oscillating monopole, which can be realized in practice by an ultrasound-driven microbubble [23]. If particles of identical densities (e.g., with $\tilde{\rho} > 1$) but different sizes are suspended in the surrounding fluid, larger particles (smaller δ) would be attracted to the bubble [23,24], whereas smaller particles would be repelled from it. The driving frequency could thus be tuned to tailor δ such that particles of different sizes experience secondary forces in opposite directions. The same principle could be applied to effect differential forces on particles of the same size but different material properties. This could be exploited to sort particles by size or material properties in microfluidic applications. The theory can also be applied to understanding particle transport in more complicated situations involving a superposition of fast oscillations and a slower steady flow; this includes streaming flows.

As an example that involves the effects of both density and compressibility contrast, we consider a polystyrene (PS) particle suspended in an acoustic plane standing wave in either water or air. In water, the effects of compressibility contrast dominate ($\tilde{\kappa} \approx 0.38$, $\tilde{\rho} \approx 1.05$) causing the particles to accumulate at pressure nodes (velocity antinodes) regardless of δ . However, density contrast effects dominate in air ($\tilde{\rho} \approx 10^3$, $\tilde{\kappa} \approx 0$), where our framework predicts that the generalized SRF focuses particles at pressure nodes for small δ , and at pressure antinodes for $\delta \gtrsim 8$. This reversal occurs due to a competition between strong inertial effects (due to large $\tilde{\rho}$) and comparably strong viscous effects (moderately large δ). Future experiments could investigate this inertioviscous transition and use it to construct acoustofluidic traps and tweezers that distinguish particle size or material properties.

In closing, we have developed a nonlinear theoretical framework for the time-averaged motion of small compressible particles in acoustic fields and oscillatory gradient flows. By generalizing the notion of secondary radiation forces and unifying it with transport by streaming, the theory self-consistently bridges inviscid acoustofluidics with viscous particle hydrodynamics. Notably, the reciprocal formulation (14) only requires a resolution of the linearized oscillation dynamics in order to rigorously quantify secondary particle motion associated with advective nonlinearities. This yields analytic insight over the entire range of Stokes layer thickness, compressibility ratio, and density ratios. The framework developed here is thus a powerful quantitative tool to understand and control the focusing, trapping, and sorting of small objects using acoustic and oscillatory driving in practical applications.

ACKNOWLEDGMENTS

We are grateful to S. Agarwal, M. Gazzola, and S. Hilgenfeldt for stimulating discussions, and thank the National Science Foundation for support through award CBET-2143943 (CAREER).

APPENDIX A: UNIFORM VALIDITY OF THE PERTURBATION EXPANSION

For steady flows, a regular perturbation expansion in particle Reynolds number does not correctly account for inertial effects far from the particle (e.g., Stokes' paradox). However, this limitation disappears for oscillating flows. To see this, we observe that for any nonzero frequency ω , unsteady inertial forces (per volume) in the Navier-Stokes equation scale as $\rho_f \omega v_1$ far away from the particle (v_1 is the local oscillatory flow scale). For large r , this inertial force dominates viscous forces, which scale as $\mu \omega v_1 / r^2$ (for $r - 1 \lesssim \delta$) or as $\mu \omega v_1 e^{-(r-1)/\delta}$ (for $r - 1 \gg \delta$) [20]. Advective inertial forces scale as $\rho_f v_1^2 / r$ far away from the particle.

We draw two important conclusions from this scaling analysis. First, the ratio of advective inertia (the leading nonlinear term) to unsteady inertia (the leading linear term) is $v_1 / (r\omega) \sim \varepsilon(a/r)$, which is small everywhere for small ε and decays with r . Second, linearized quantities oscillate with frequency ω , whereas secondary nonlinear quantities involve a steady term ("zero frequency oscillations") and terms oscillating with a frequency of 2ω , but contain no components at frequency ω . Both (i) the uniform smallness of advective inertia relative to unsteady inertia, and (ii) the separation of nonlinear and linear dynamics in frequency space, ensure that the regular perturbation expansion is valid up to $O(\varepsilon^2)$. Both arguments break down for steady viscous flows ($\omega = 0$) leading to the far-field inertial effects that characterize steady flows at small (but finite) Reynolds numbers. In the present framework, we estimate that these effects only enter at $O(\varepsilon^3)$ or $O(\varepsilon^4)$, corresponding to Saffman-like and Oseen-like wakes, respectively, in the time-averaged flow.

APPENDIX B: EFFECTIVE BOUNDARY CONDITIONS

We denote a material point on the instantaneous particle surface $S_p(t)$ by $\mathbf{X}(t)$, so the no-slip condition is $d\mathbf{X}/dt = \varepsilon \mathbf{v}(\mathbf{X}(t), t)$. We split $\mathbf{X}(t)$ into a time-averaged part $\langle \mathbf{X} \rangle$ [which lies on the mean particle surface $\langle S_p \rangle$] and varies slowly over timescale $(\varepsilon^2 \omega)^{-1}$ as the particle moves due

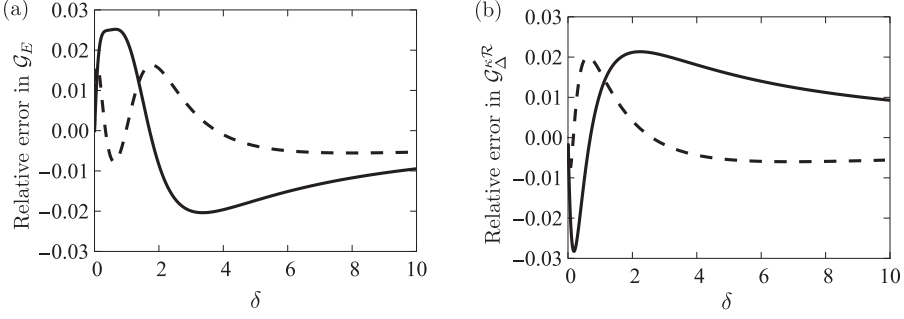


FIG. 5. Relative errors between approximations in (19) and exact coefficients for (a) \mathcal{G}_E and (b) $\mathcal{G}_\Delta^{\kappa\mathcal{R}}$, showing real (solid) and imaginary (dashed) parts.

to secondary forces], and an oscillating part $\varepsilon\xi(\langle\mathbf{X}\rangle, t)$, so that $\mathbf{X}(t) = \langle\mathbf{X}\rangle + \varepsilon\xi(\langle\mathbf{X}\rangle, t)$. Writing $\mathbf{v} \sim \mathbf{v}_1 + \varepsilon\mathbf{v}_2$ and Taylor expanding for small ε leads to

$$\frac{d\langle\mathbf{X}\rangle}{dt} + \varepsilon\frac{d\xi}{dt} = \varepsilon\mathbf{v}_1(\langle\mathbf{X}\rangle, t) + \varepsilon^2\mathbf{v}_2(\langle\mathbf{X}\rangle, t) + \varepsilon^2\xi(\langle\mathbf{X}\rangle, t) \cdot \nabla\mathbf{v}_1(\langle\mathbf{X}\rangle, t) + O(\varepsilon^3). \quad (\text{B1})$$

Grouping oscillating and steady components yields

$$\frac{d\xi}{dt} = \mathbf{v}_1, \quad \frac{d\langle\mathbf{X}\rangle}{dt} = \varepsilon^2\langle\mathbf{v}_2 + \xi \cdot \nabla\mathbf{v}_1\rangle. \quad (\text{B2})$$

The primary surface displacement is therefore $\xi(\langle\mathbf{X}\rangle, t) = \int \mathbf{v}_1(\langle\mathbf{X}\rangle, t) dt$. Identifying $d\xi/dt$ and $d\langle\mathbf{X}\rangle/dt$ on the left sides of (B2) with the oscillatory and steady kinematics of the particle, respectively, yields (3) of the main text.

APPENDIX C: FORCE COEFFICIENTS

Exact expressions for the force coefficients \mathcal{G}_E and $\mathcal{G}_\Delta^{\kappa\mathcal{R}}$ are

$$\begin{aligned} \mathcal{G}_E = & -\frac{1}{640\lambda^2(\lambda+1)}(i\lambda^8 + (1+6i)\lambda^7 + (6+31i)\lambda^6 - (93-51i)\lambda^5 + (147+108i)\lambda^4 \\ & + 252(1-i)\lambda^3 + (732+1152i)\lambda^2 + (1440+1152i)\lambda + 1440) \\ & -\frac{3\lambda^2(\lambda^2+3i\lambda-3)}{32(\lambda+1)}e^\lambda E_1(\lambda) + \frac{\lambda^2(\lambda^5+6\lambda^4+33\lambda^3+123\lambda^2+270\lambda+270)}{640(\lambda+1)}e^{-i\lambda} E_1(-i\lambda) \\ & -\frac{3\lambda^2(\lambda^2+9)}{16(\lambda+1)}e^{(1-i)\lambda} E_1((1-i)\lambda), \end{aligned} \quad (\text{C1a})$$

$$\mathcal{G}_\Delta^{\kappa\mathcal{R}} = \frac{(i\lambda^5 + \lambda^4 - 14i\lambda^3 - 18\lambda^2 + 48i\lambda - 48)}{64\lambda^2} - \frac{\lambda^2(\lambda^2 - 12)}{64}e^{-i\lambda} E_1(-i\lambda), \quad (\text{C1b})$$

where $E_1(z) = \int_1^\infty t^{-1}e^{-zt} dt$ is an exponential integral [defined for $\text{Re}(z) > 0$]. Figure 5 shows relative errors between the approximations (19a) and (19d) and exact expressions (C1); errors are $<3\%$ for all δ .

-
- [1] H. Bruus, *Acoustofluidics 7: The acoustic radiation force on small particles*, *Lab Chip* **12**, 1014 (2012).
 [2] N. Riley, *Steady streaming*, *Annu. Rev. Fluid. Mech.* **33**, 43 (2001).

- [3] J. Friend and L. Y. Yeo, Microscale acoustofluidics: Microfluidics driven via acoustics and ultrasonics, *Rev. Mod. Phys.* **83**, 647 (2011).
- [4] P. Marmottant and S. Hilgenfeldt, Controlled vesicle deformation and lysis by single oscillating bubbles, *Nature (London)* **423**, 153 (2003).
- [5] B. R. Mutlu, J. F. Edd, and M. Toner, Oscillatory inertial focusing in infinite microchannels, *Proc. Natl. Acad. Sci. USA* **115**, 7682 (2018).
- [6] S. Yang, Z. Tian, Z. Wang, J. Rufo, P. Li, J. Mai, J. Xia, H. Bachman, P.-H. Huang, M. Wu *et al.*, Harmonic acoustics for dynamic and selective particle manipulation, *Nat. Mater.* **21**, 540 (2022).
- [7] J. Rufo, F. Cai, J. Friend, M. Wiklund, and T. J. Huang, Acoustofluidics for biomedical applications, *Nat. Rev. Methods Primers* **2**, 30 (2022).
- [8] D. Klotsa, K. A. Baldwin, R. J. A. Hill, R. M. Bowley, and M. R. Swift, Propulsion of a two-sphere swimmer, *Phys. Rev. Lett.* **115**, 248102 (2015).
- [9] D. Foresti and D. Poulidakos, Acoustophoretic contactless elevation, orbital transport and spinning of matter in air, *Phys. Rev. Lett.* **112**, 024301 (2014).
- [10] V. Lee, N. M. James, S. R. Waitukaitis, and H. M. Jaeger, Collisional charging of individual submillimeter particles: Using ultrasonic levitation to initiate and track charge transfer, *Phys. Rev. Mater.* **2**, 035602 (2018).
- [11] M. A. Andrade, A. Marzo, and J. C. Adamowski, Acoustic levitation in mid-air: Recent advances, challenges, and future perspectives, *Appl. Phys. Lett.* **116**, 250501 (2020).
- [12] R. Lirette, J. Mobley, and L. Zhang, Ultrasonic extraction and manipulation of droplets from a liquid-liquid interface with near-field acoustic tweezers, *Phys. Rev. Appl.* **12**, 061001 (2019).
- [13] Y. Chen, Z. Fang, B. Merritt, D. Strack, J. Xu, and S. Lee, Onset of particle trapping and release via acoustic bubbles, *Lab Chip* **16**, 3024 (2016).
- [14] R. Thameem, B. Rallabandi, and S. Hilgenfeldt, Fast inertial particle manipulation in oscillating flows, *Phys. Rev. Fluids* **2**, 052001 (2017).
- [15] G. A. Voth, B. Bigger, M. Buckley, W. Losert, M. Brenner, H. A. Stone, and J. Gollub, Ordered clusters and dynamical states of particles in a vibrated fluid, *Phys. Rev. Lett.* **88**, 234301 (2002).
- [16] D. Klotsa, M. R. Swift, R. M. Bowley, and P. J. King, Chain formation of spheres in oscillatory fluid flows, *Phys. Rev. E* **79**, 021302 (2009).
- [17] M. X. Lim, A. Souslov, V. Vitelli, and H. M. Jaeger, Cluster formation by acoustic forces and active fluctuations in levitated granular matter, *Nat. Phys.* **15**, 460 (2019).
- [18] L. P. Gor'kov, Forces acting on a small particle in an acoustic field within an ideal fluid, *Dokl. Akad. Nauk SSSR* **140**, 88 (1961).
- [19] L. V. King, On the acoustic radiation pressure on spheres, *Proc. R. Soc. London A* **147**, 212 (1934).
- [20] M. Settnes and H. Bruus, Forces acting on a small particle in an acoustical field in a viscous fluid, *Phys. Rev. E* **85**, 016327 (2012).
- [21] R. Gatignol, The Faxén formulae for a rigid particle in an unsteady non-uniform Stokes flow, *J. Mec. Theor. Appl.* **2**, 143 (1983).
- [22] M. R. Maxey and J. J. Riley, Equation of motion for a small rigid sphere in a nonuniform flow, *Phys. Fluids* **26**, 883 (1983).
- [23] K. Chong, S. D. Kelly, S. Smith, and J. D. Eldredge, Inertial particle trapping in viscous streaming, *Phys. Fluids* **25**, 033602 (2013).
- [24] S. Agarwal, B. Rallabandi, and S. Hilgenfeldt, Inertial forces for particle manipulation near oscillating interfaces, *Phys. Rev. Fluids* **3**, 104201 (2018).
- [25] S. Agarwal, G. Upadhyay, Y. Bhosale, M. Gazzola, and S. Hilgenfeldt, Density-contrast induced inertial forces on particles in oscillatory flows, [arXiv:2308.04423](https://arxiv.org/abs/2308.04423).
- [26] A. A. Doinikov, Acoustic radiation pressure on a compressible sphere in a viscous fluid, *J. Fluid Mech.* **267**, 1 (1994).
- [27] S. Danilov and M. Mironov, Mean force on a small sphere in a sound field in a viscous fluid, *J. Acoust. Soc. Am.* **107**, 143 (2000).
- [28] S. Kim and S. J. Karrila, *Microhydrodynamics: Principles and Selected Applications* (Butterworth-Heinemann, Boston, USA, 1991).

- [29] C. Pozrikidis, *Boundary Integral and Singularity Methods for Linearized Viscous Flow* (Cambridge University Press, New York, 1992).
- [30] H. A. Stone and A. D. Samuel, Propulsion of microorganisms by surface distortions, [Phys. Rev. Lett. **77**, 4102 \(1996\)](#).
- [31] H. Masoud and H. A. Stone, The reciprocal theorem in fluid dynamics and transport phenomena, [J. Fluid Mech. **879**, P1 \(2019\)](#).
- [32] N. Oppenheimer, S. Navardi, and H. A. Stone, Motion of a hot particle in viscous fluids, [Phys. Rev. Fluids **1**, 014001 \(2016\)](#).
- [33] F. Nadal and E. Lauga, Small acoustically forced symmetric bodies in viscous fluids, [J. Acoust. Soc. Am. **139**, 1081 \(2016\)](#).
- [34] S. Agarwal, F. K. Chan, B. Rallabandi, M. Gazzola, and S. Hilgenfeldt, An unrecognized inertial force induced by flow curvature in microfluidics, [Proc. Natl. Acad. Sci. USA **118**, e2103822118 \(2021\)](#).
- [35] B. Rallabandi, Inertial forces in the Maxey–Riley equation in nonuniform flows, [Phys. Rev. Fluids **6**, L012302 \(2021\)](#).